

ORIGINAL ARTICLE

Open Access



Testing the Coulomb stress triggering hypothesis for three recent megathrust earthquakes

Takeo Ishibe^{1*}, Yoshiko Ogata^{2,3}, Hiroshi Tsuruoka² and Kenji Satake²

Abstract

We test the static Coulomb stress triggering hypothesis for three recent megathrust earthquakes (the 2004 Sumatra–Andaman earthquake, the 2010 Maule earthquake, and the 2011 Tohoku–Oki earthquake) using focal mechanism solutions for actual earthquakes as receiver faults to calculate Coulomb stress changes. For the 2004 Sumatra–Andaman and 2011 Tohoku–Oki earthquakes, the median values of the Coulomb stress changes for 100 consecutive earthquakes revealed temporal changes from approximately zero before the megathrust earthquake to significant positive values following the mainshock, followed by decay over time. Furthermore, the ratio of the number of positively to negatively stressed receiver faults increased after the megathrust. These results support the triggering hypothesis that the static stress changes imparted by megathrust earthquakes cause seismicity changes. This is in contrast to the results of a previous study that used optimally orientated receiver faults to calculate Coulomb stress changes, and this difference indicates the importance of considering the spatial and temporal heterogeneities of receiver fault distributions. For the 2010 Maule earthquake, however, the results are strongly dependent on fault-slip models. Since most receiver faults are concentrated in the mainshock source region, slip models significantly affect the computed Coulomb stress changes and sometimes cause anomalous stress concentrations along the edge of each sub-fault.

Keywords: Coulomb stress changes, 2004 Sumatra–Andaman earthquake, 2010 Maule earthquake, 2011 Tohoku–Oki earthquake, Heterogeneity of receiver fault mechanisms

Background

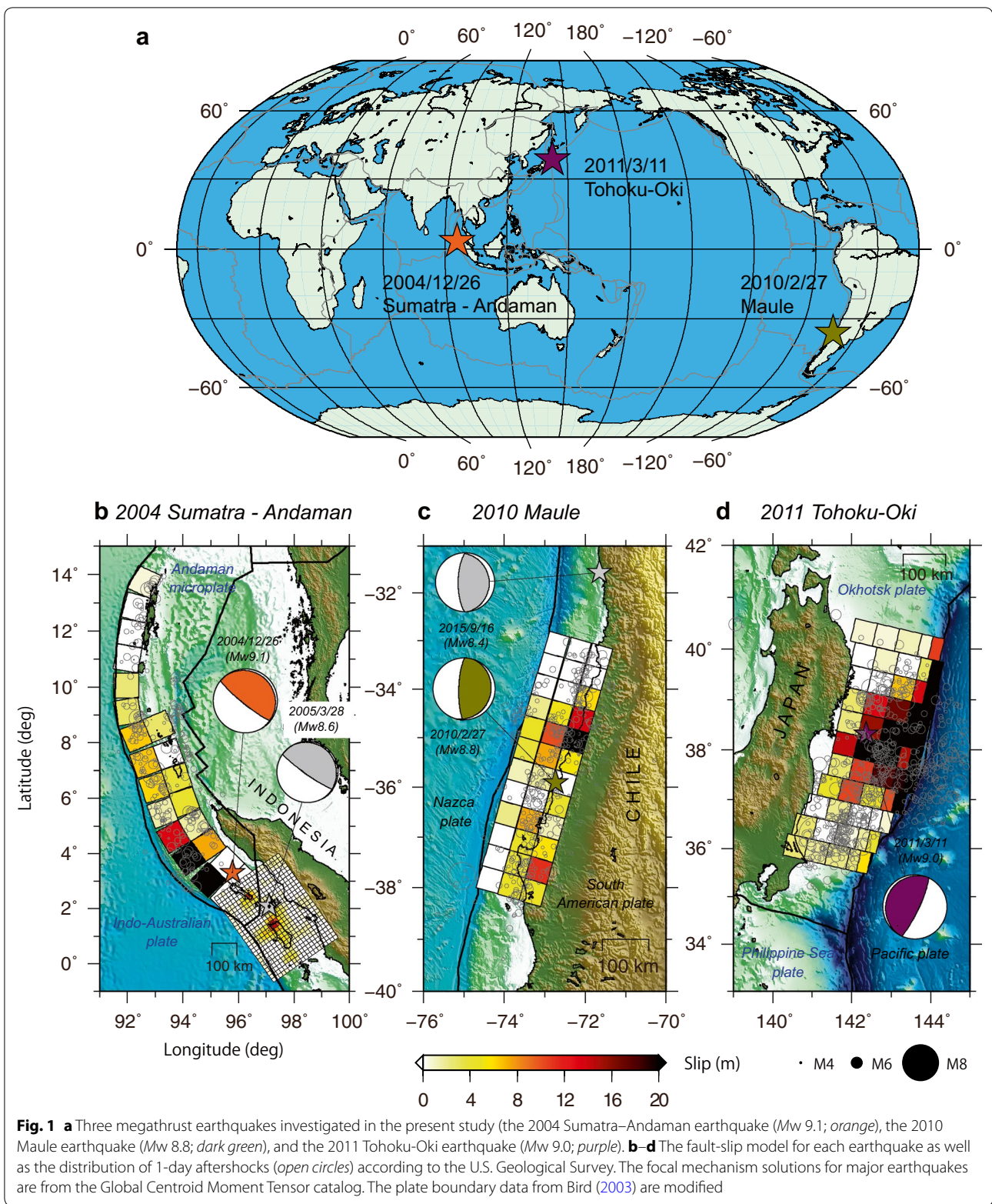
Earthquake triggering and seismicity rate changes following large or great earthquakes have been discussed in terms of static (and/or dynamic) changes in the Coulomb failure function (ΔCFF) (Harris and Simpson 1992; Stein et al. 1992, 1994; Reasenber and Simpson 1992; Hill et al. 1993; Anderson et al. 1994; Toda et al. 1998; Ogata 2007; Chan and Stein 2009; Chan et al. 2016). The ΔCFF is defined as $\Delta CFF = \Delta\tau - \mu'\Delta\sigma$, where $\Delta\tau$ is the shear stress change on a given failure plane (assumed to be positive in the fault-slip direction), $\Delta\sigma$ is the normal stress change (assumed to be positive in the compressive direction), and μ' is the apparent coefficient of friction.

Positive ΔCFF values enhance failures, whereas negative values suppress failures.

Three megathrust earthquakes, the 2004 Sumatra–Andaman earthquake (M_w 9.1; U. S. Geological Survey), the 2010 Maule earthquake (M_w 8.8), and the 2011 Tohoku–Oki earthquake (M_w 9.0), provided us a great opportunity to investigate the triggering hypothesis that co-seismic stress changes transferred from large earthquakes cause seismicity changes (Fig. 1). For the Tohoku–Oki earthquake, Toda et al. (2011) showed that there is a mean 47% gain in positively stressed aftershock mechanisms over background (1997–2011 March 10) earthquakes. Furthermore, Ishibe et al. (2015) showed that the ΔCFF values following the Tohoku–Oki earthquake have a statistically higher ratio of positively stressed receiver faults compared to those before the Tohoku–Oki earthquake.

*Correspondence: ishibe@erc.adeq.or.jp

¹ Association for the Development of Earthquake Prediction, 1-5-18, Sarugaku-cho, Chiyoda-ku, Tokyo 101-0064, Japan
Full list of author information is available at the end of the article



Recently, Miao and Zhu (2012) compared the spatial distribution of the Δ CFF imparted by the above three megathrust earthquakes with their aftershock distributions by assuming optimally orientated faults to be receiver faults, and concluded that there is no clear evidence that the Coulomb stress changes enhanced the aftershock activity. The ratios of aftershocks that occurred in the positively stressed regions following the Sumatra–Andaman, Maule, and Tohoku–Oki earthquakes were 47.6, 49.8, and 47.0%, respectively. They reported that the static triggering hypothesis worked well, with more than 85% of aftershocks having positive Δ CFF values, for the two large intraplate earthquakes (the 1999 Chi–Chi and 2008 Wenchuan earthquakes).

Assumption of the receiver fault mechanism sometimes greatly affects estimation of the Δ CFF. The simplest way to assume the specified receiver fault is to fix the strike, dip angle, and rake angle, but this method is valid either for major source faults with well-known fault geometries or a region with a spatially and temporally homogeneous stress field. Another way is to assume optimally oriented receiver faults, which are determined so as to maximize the Δ CFF under the specified local/regional stress field (King et al. 1994). This can also produce large errors in a complex regional stress field in which earthquakes with various focal mechanisms occur, unless the heterogeneity of the local/regional stress field is properly considered.

In the present study, we calculate the Δ CFF for nodal planes of focal mechanism solutions for actual earthquakes. This method has been proven to be effective in reducing the uncertainty of receiver faults in heterogeneous stress fields (Hardebeck et al. 1998; Imanishi et al. 2006; Toda 2008; Ishibe et al. 2011a, b, 2015; Enescu et al. 2012; Heidarzadeh et al. 2016). Following the recent occurrence of megathrust earthquakes, drastic changes in focal mechanism solutions from dominant thrust-type to a variety of types have been observed (e.g. Lay et al. 2005; Asano et al. 2011; Nettles et al. 2011). We investigate the correlation between the Coulomb stress changes transferred from three megathrust earthquakes and seismicity changes before and after the megathrust earthquakes in the neighboring regions.

Data and methodology

We use variable-slip models obtained from tsunami waveforms for the three megathrust earthquakes [the 2004 Sumatra–Andaman earthquake (Fujii and Satake 2007), the 2010 Maule earthquake (Fujii and Satake 2013), and the 2011 Tohoku–Oki earthquake (Satake et al. 2013)] (Fig. 1). In order to examine the sensitivity of Δ CFF computation to slip models, we also use the variable-slip models proposed by Rhie et al. (2007) and Ammon et al. (2005) for the Sumatra–Andaman

earthquake, by Delouis et al. (2010) and Luttrell et al. (2011) for the Maule earthquake, and by Yokota et al. (2011) and Gusman et al. (2012) for the Tohoku–Oki earthquake (Additional file 1: Figure S1). For the case of the Sumatra–Andaman earthquake, we include the Δ CFF due to the *M*w 8.5 Nias earthquake that occurred in March 2005 southeast of the 2004 source region using the fault-slip model obtained from teleseismic body-wave inversion (Konca et al. 2007).

For receiver faults on which stress changes are calculated, we use the focal mechanism solutions of earthquakes between January 1, 1976 and September 31, 2015 obtained from the Global Centroid Moment Tensor (GCMT) catalog (e.g. Ekström et al. 2012) (Additional file 2: Figure S2). For the case of the Tohoku–Oki earthquake, we also use the F-net focal mechanisms provided by the National Research Institute for Earth Science and Disaster Resilience (Fukuyama et al. 1998). We grouped these mechanisms into pre-seismic and post-seismic periods, before and after the occurrence of the megathrust earthquakes. The number of earthquakes we used to compute the Δ CFF values was 1374 for the Sumatra–Andaman earthquake, 436 for the Maule earthquake, and 1537 for the Tohoku–Oki earthquake. Even if a majority of aftershock nodal planes were positively stressed by the mainshock rupture, this would not necessarily prove the stress triggering hypothesis because the distribution of receiver faults is controlled primarily by predominant stress fields. Thus, we evaluate the triggering hypothesis by comparing the calculated Coulomb stress changes after the megathrusts to those during pre-seismic periods as background.

We calculate the Δ CFF values for two nodal planes of each focal mechanism solution. We assume an elastic half-space with a shear modulus of 40 GPa and a Poisson's ratio of 0.25. For the apparent friction coefficient (μ'), we adopt an empirically introduced value, $\mu' = 0.4$, but we also repeat our analyses for two other values ($= 0.1$ and 0.8). Laboratory rock experiments on frictional slip indicate higher values, e.g., $0.5 \leq \mu' \leq 0.8$ (e.g., Byerlee and Brace 1968), whereas fluid injection decreases the apparent friction coefficient when the pore–fluid pressure increases (Skempton 1954).

We calculate the median Δ CFF value for receiver faults for 100 consecutive earthquakes by moving the time window for 50 earthquakes. The Δ CFF values for the two nodal planes differ because the unclamping stresses are not the same, but we do not know which of these is the actual receiver fault. In order to consider the arbitrariness of nodal plane selection, we conduct a Monte Carlo simulation in which either the first or the second nodal plane of each focal mechanism solution is randomly selected as a receiver fault. In each time-window, we create 1000

datasets and calculate the average and standard deviation of the median Δ CFF values. We also calculate the ratios of three cases in which (1) both nodal planes are positively stressed; (2) one nodal plane is positively stressed, while the other is negatively stressed; and (3) both nodal planes are negatively stressed. We then evaluate the Coulomb index, which is the ratio of the number of receiver faults with stress increases for at least one nodal plane (e.g., Hardebeck et al. 1998) during both the pre-seismic and post-seismic periods.

Results and discussion

Figure 2 shows the distribution of the Δ CFF values and the focal mechanism solutions during the pre-seismic and post-seismic periods. One of the characteristics of the focal mechanism distribution during the post-seismic period is activation of normal-faulting earthquakes in the shallow crustal region of the overriding plate and the outer-rise region. For the case of the Tohoku-Oki earthquake, shallow normal-faulting earthquakes abruptly began to occur in the Ibaraki/Fukushima prefectural boundary area (coastal region around 37 °N) (e.g., Kato et al. 2011) and the outer-rise region along the Japan Trench. Similar normal-faulting earthquake sequences were also reported for the other two megathrust earthquakes: the Pichilemu region (around 34.5 °S) along the Chilean coast after the Maule earthquake (e.g., Fariás et al. 2011) and East offshore of the Nicobar Islands (around 8 °N) after the Sumatra–Andaman earthquake (e.g., Lay et al. 2005; Dewey et al. 2007). Most of these normal-faulting earthquakes were positively stressed due to the occurrence of the megathrust earthquakes.

The temporal changes in the median Δ CFF values for the three megathrust earthquakes are shown in Fig. 3. Here, we focused on the temporal changes since 2000, because the temporal changes during the pre-seismic periods are negligibly small. (See Additional file 3: Figure S3, Additional file 4: Figure S4 for temporal changes in the median Coulomb stress change after January 1976.) The median values of Δ CFF are several bars during post-seismic periods, whereas they are approximately zero during pre-seismic periods for the Sumatra–Andaman and Tohoku-Oki earthquakes (Fig. 3). The rapidly increased median Δ CFF values gradually decayed to background levels for the Sumatra–Andaman earthquake. However, these were still elevated 4 years after the Tohoku-Oki earthquake. The decay rate became smaller approximately 3 years after the mainshock, suggesting that factors other than Coulomb stress changes, which will be discussed later, also contributed to keep the median Δ CFF elevated (e.g., Toda and Stein 2013).

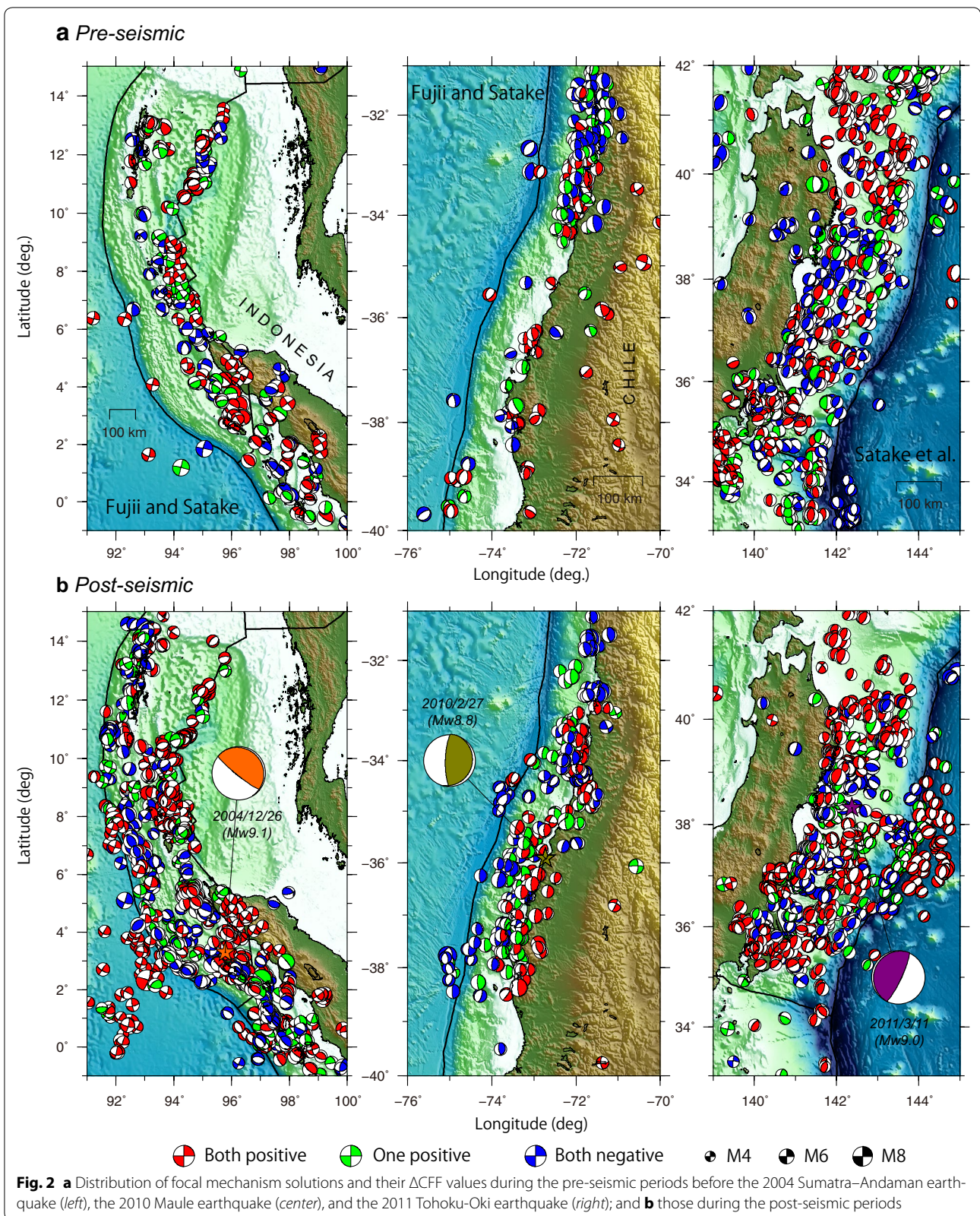
The Coulomb index during the post-seismic period was greater than 50%, with the exception of one of the

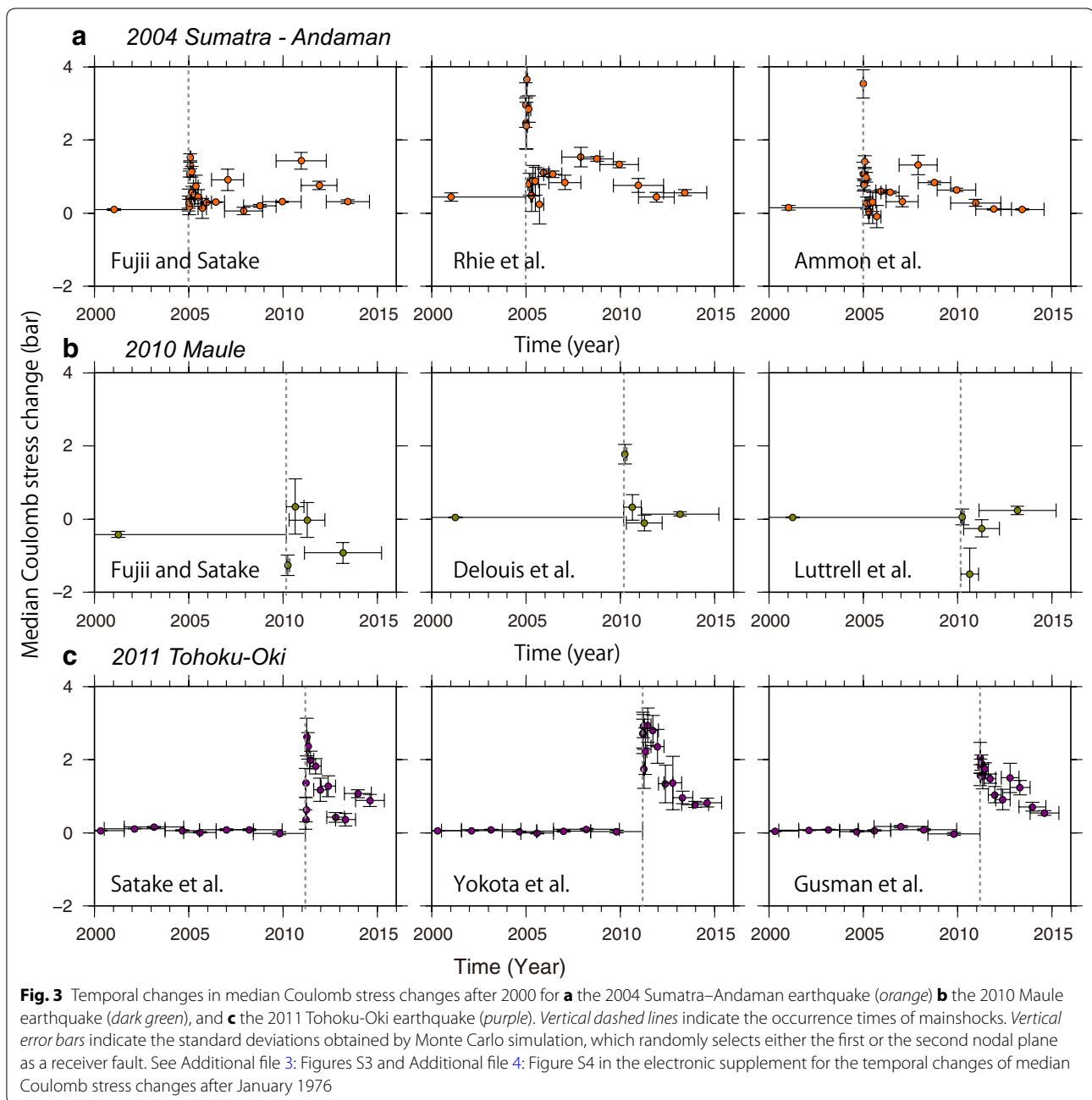
27 cases (Table 1). These results are inconsistent with those of a previous study, in which the seismicity was determined to be less than 50% in the positively stressed region by assuming an optimally oriented receiver fault. For 19 cases out of 27 cases, the Coulomb index was higher during the post-seismic period than that during the pre-seismic period. For example, using the fault model of Yokota et al. (2011) with an apparent coefficient friction of 0.4, 79.3% of receiver faults were positively stressed for at least one nodal plane following the Tohoku-Oki earthquake, whereas 64.2% of receiver faults were positive during the pre-seismic period. This is consistent with the findings of previous studies (e.g., Toda et al. 2011; Ishibe et al. 2015).

For the Maule earthquake, however, temporal changes in the median Δ CFF exhibit various patterns depending on the slip model: an abrupt increase in median Δ CFF value for the slip model of Delouis et al. (2010), an abrupt decrease for that of Fujii and Satake (2013), and almost no change for that of Luttrell et al. (2011). Most of the receiver faults used to compute the Δ CFF for the 2010 Maule earthquake were interplate aftershocks with a thrust mechanism and were concentrated in the mainshock source region (see Additional file 5: Figure S5). The evaluated Δ CFF for these receiver faults may include large uncertainties because slip models using rectangular sub-faults artificially cause anomalous stress concentrations along the edge of each sub-fault (e.g., Woessner et al. 2012), and hence the computed median values are strongly affected by these anomalous values near the source. Another possible reason is the smaller number of available receiver faults compared with the other two megathrust earthquakes.

In order to examine the sensitivity of the Δ CFF calculation to the slip model and the assumed value of the apparent friction coefficient, we repeated our analyses for other slip models (see Additional files 6, 7, 8, 9, 10, 11, 12: Figures S6 through S12) and two other apparent friction coefficients ($\mu' = 0.1$ and 0.8). The computed Δ CFF value is insensitive to the slip model for the Tohoku-Oki and Sumatra–Andaman earthquakes. The temporal change in the Δ CFF is similar for different values of the friction coefficient, i.e., the abrupt increase in the median value following the occurrence of a megathrust earthquake and the gradual decay toward the background level.

The catalog dependency of our results was also tested for the case of the Tohoku-Oki earthquake by using F-net focal mechanisms as receiver faults. Figure 4 shows the distribution of the receiver faults with the calculated Δ CFF and the temporal changes in the median Δ CFF value using the fault-slip model of Yokota et al. (2011) with $\mu' = 0.4$. (see Additional file 13: Figure S13, Additional file 14: Figure S14 for





different apparent coefficients of friction). The median ΔCFF exhibited similar temporal changes associated with the Tohoku-Oki earthquake: a sudden increase followed by a gradual decrease toward the background level. The median ΔCFF fluctuates more for the F-net catalog than for the GCMT catalog. This may reflect the characteristics of earthquake clustering, because the F-net data include a much larger number of focal mechanism solutions than the GCMT catalog.

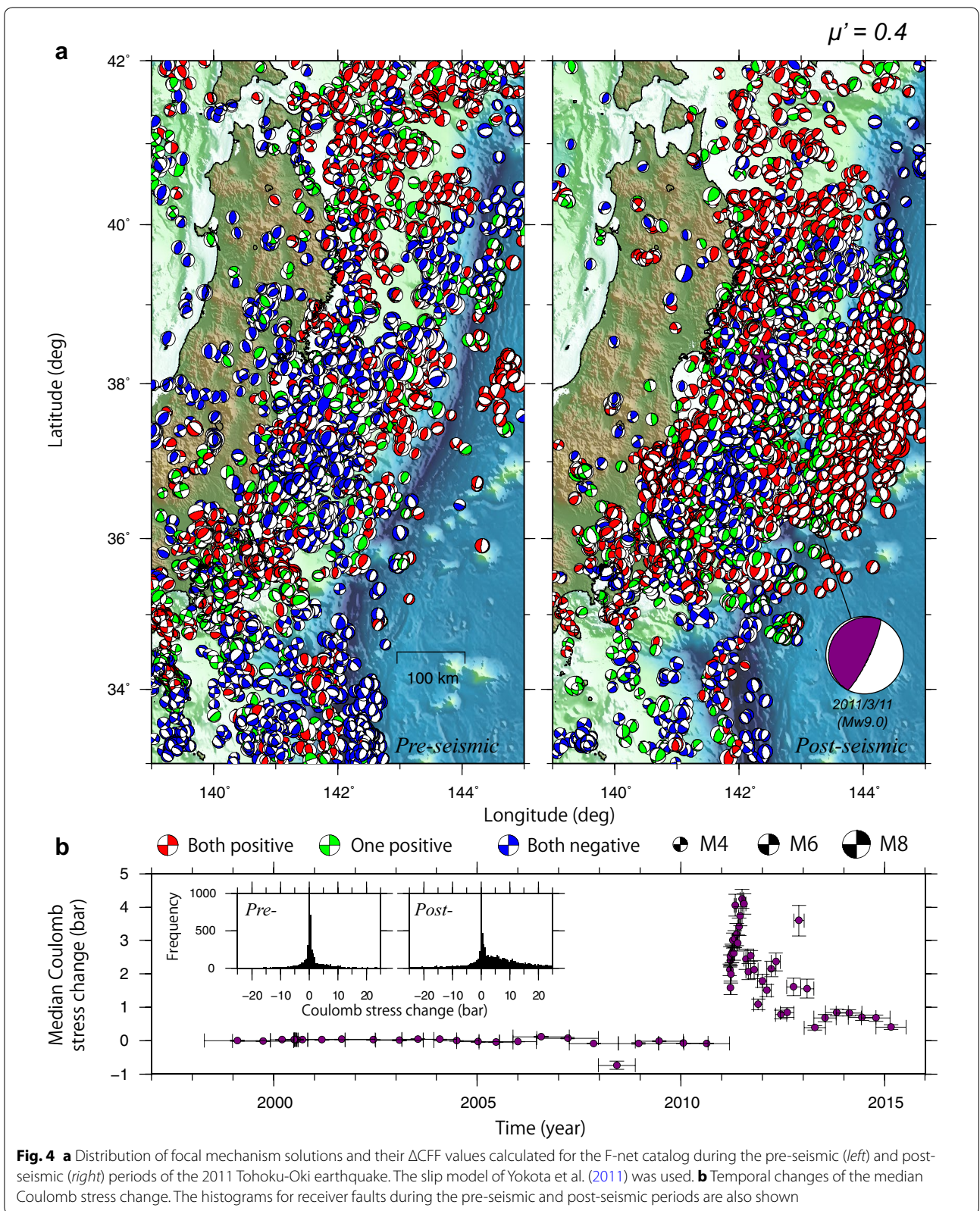
Concluding remarks and future developments

We investigated the correlation between static Coulomb stress changes imparted by three megathrust earthquakes and changes in focal mechanism solutions by means of abundant focal mechanism solutions of earthquake catalogs as receiver faults. The median Coulomb stress was approximately zero during the pre-seismic period before the megathrust earthquake, abruptly increased as a result of the earthquake, and then gradually decreased,

Table 1 Ratios of receiver faults during the pre-seismic and post-seismic periods with different apparent coefficients of friction and fault-slip models

Event	Model	μ'	Pre-seismic period				Post-seismic period			
			Both positive (%)	One positive (%)	Both negative (%)	Coulomb index (%)	Both positive (%)	One positive (%)	Both negative (%)	Coulomb index (%)
2004 Sumatra–Andaman	Fujii and Satake (2007)	0.1	56.3	7.4	36.4	63.7	57.1	4.5	38.5	61.6
		0.4	51.1	23.4	25.5	74.5	56.1	17.6	26.3	73.7
		0.8	48.5	35.9	15.6	84.4	54.1	26.0	19.9	80.1
		0.1	49.8	6.5	43.7	56.3	59.4	5.8	34.9	65.2
		0.4	51.5	14.7	33.8	66.2	57.9	17.2	24.9	75.1
2010 Maule	Ammon et al. (2005)	0.8	55.0	20.3	24.7	75.3	56.6	25.9	17.5	82.5
		0.1	45.9	6.5	47.6	52.4	53.0	5.9	41.1	58.9
		0.4	48.5	19.5	32.0	68.0	53.2	20.9	25.9	74.1
		0.8	51.1	27.7	21.2	78.8	56.8	27.0	16.2	83.8
		0.1	37.4	7.6	55.0	45.0	41.0	3.0	56.0	44.0
2011 Tohoku–Oki	Fujii and Satake (2013)	0.4	30.4	22.2	47.4	52.6	33.1	24.1	42.9	57.2
		0.8	25.7	31.6	42.7	57.3	27.1	34.2	38.7	61.3
		0.1	66.7	2.3	31.0	69.0	57.5	4.9	37.6	62.4
		0.4	50.3	22.8	26.9	73.1	53.0	17.3	29.7	70.3
		0.8	26.3	48.5	25.1	74.8	41.4	34.2	24.4	75.6
2011 Tohoku–Oki	Luttrell et al. (2011)	0.1	66.1	2.9	31.0	69.0	48.1	5.3	46.6	53.4
		0.4	45.6	25.1	29.2	70.7	46.6	18.4	35.0	65.0
		0.8	23.4	38.0	38.6	61.4	39.5	32.7	27.8	72.2
		0.1	65.3	3.7	31.0	69.0	68.5	4.2	27.3	72.7
		0.4	50.4	20.1	29.5	70.5	57.8	18.0	24.2	75.8
2011 Tohoku–Oki	Satake et al. (2013)	0.8	38.1	33.7	28.2	71.8	48.9	26.4	24.6	75.3
		0.1	56.7	5.1	38.2	61.8	68.5	5.1	26.4	73.6
		0.4	46.4	17.8	35.8	64.2	60.3	19.0	20.7	79.3
		0.8	35.8	31.3	32.9	67.1	52.9	27.4	19.7	80.3
		0.1	67.5	3.7	28.8	71.2	72.6	4.1	23.3	76.7
2011 Tohoku–Oki	Gusman et al. (2012)	0.4	49.2	24.8	26.0	74.0	64.0	18.7	17.3	82.7
		0.8	30.6	43.8	25.6	74.4	53.2	30.4	16.5	83.6

The underlined/italic numbers indicate that the Coulomb index during the post-seismic period increased/decreased compared to that during the pre-seismic period



at least for the Sumatra–Andaman and Tohoku–Oki earthquakes. The ratio of positively to negatively stressed receiver faults increased following these megathrust earthquakes for almost all slip models and apparent friction coefficient values. Changes in the focal mechanism distribution that can be correlated with static Coulomb stress changes due to megathrust earthquakes support the static stress triggering hypothesis. The conclusion of the present study is opposite that of a previous study using optimally orientated receiver faults, and this difference indicates the importance of considering the spatial and temporal heterogeneities of receiver faults.

In the present study, we considered only the static stress changes transferred from co-seismic fault slips of the mainshocks. However, other possible factors for triggering seismicity changes, such as dynamic stress change due to the passage of seismic waves (e.g., Hill et al. 1993; Miyazawa 2011), a decrease in failure strength due to an increase in pore–fluid pressure (e.g., Hubbert and Rubey 1959), post-seismic slip, static stress change from indirectly triggered earthquakes by numerous aftershocks, acceleration of relative plate motion (e.g., Heki and Mitsui 2013; Uchida et al. 2016), and/or viscoelastic relaxation (e.g., Pollitz and Sacks 1995), have been suggested by various studies. These might disturb or mask the correlation between Coulomb stress changes co-seismically transferred from the mainshocks and changes in seismicity following the occurrence of mainshocks.

Additional files

Additional file 1: Figure S1. Slip distribution for the three megathrust earthquakes used in the present study: (a) the 2004 Sumatra–Andaman earthquake, (b) the 2010 Maule earthquake, and (c) the 2011 Tohoku–Oki earthquake.

Additional file 2: Figure S2. Distribution of focal mechanism solutions of earthquakes during the (a) pre-seismic and (b) post-seismic periods for three megathrust earthquakes. The colors in the dilatation of the lower hemisphere indicate focal depths.

Additional file 3: Figure S3. Temporal variation in the median Coulomb stress change since January 1976 for (a) the 2004 Sumatra–Andaman earthquake (orange), (b) the 2010 Maule earthquake (dark green), and (c) the 2011 Tohoku–Oki earthquake (purple). The vertical dashed lines indicate the occurrence times of mainshocks. The vertical error bars indicate the standard deviations obtained through the Monte Carlo simulation, which randomly selects either the first or second nodal plane as a receiver fault.

Additional file 4: Figure S4. Temporal changes of the median Coulomb stress change since January 1976 for the 2004 Sumatra–Andaman (orange), 2010 Maule (dark green), and 2011 Tohoku–Oki (purple) earthquakes with apparent coefficients of (a) 0.1 and (b) 0.8.

Additional file 5: Figure S5. Types of focal mechanism solutions for earthquakes in each region during (a) the pre-seismic period and (b) the post-seismic period. The pie charts at the upper right show the ratios of each focal mechanism type (red: thrust, green: strike-slip, blue: normal, and grey: oblique-slip).

Additional file 6: Figure S6. Spatial distribution of receiver faults with calculated Coulomb stress change imparted by the 2004 Sumatra–Andaman and 2005 Nias earthquakes. The red, green, and blue focal spheres show the positively stressed receiver faults for both nodal planes, the positively stressed receiver faults for either the first or second nodal plane, and the negatively stressed receiver faults for both nodal planes.

Additional file 7: Figure S7. Spatial distribution of receiver faults with calculated Coulomb stress change imparted by the 2010 Maule earthquake. The symbols are as described in Figure S6.

Additional file 8: Figure S8. Spatial distribution of receiver faults with calculated Coulomb stress change imparted by the 2011 Tohoku–Oki earthquake. The symbols are as described in Figure S6.

Additional file 9: Figure S9. Temporal distribution of the calculated Coulomb stress change imparted by the 2004 Sumatra–Andaman and 2005 Nias earthquakes for three different apparent coefficients and slip models [slip models of (a) Fujii and Satake (2007), (b) Rhie et al. (2007), and (c) Ammon et al. (2005)]. The colors indicate the hypocentral depths of the receiver faults.

Additional file 10: Figure S10. Temporal distribution of calculated Coulomb stress change imparted by the 2010 Maule earthquake for three different apparent coefficients and slip models [slip models of (a) Fujii and Satake (2013), (b) Delouis et al. (2010), and (c) Luttrell et al. (2011)]. The colors indicate the hypocentral depths of the receiver faults.

Additional file 11: Figure S11. Temporal distribution of the calculated Coulomb stress change imparted by the 2011 Tohoku–Oki earthquake for three different apparent coefficients and slip models [slip models of (a) Satake et al. (2013), (b) Yokota et al. (2011), and (c) Gusman et al. (2012)]. The colors indicate the hypocentral depths of the receiver faults.

Additional file 12: Figure S12. Temporal variation in the median Coulomb stress change for the 2004 Sumatra–Andaman, 2010 Maule, and 2011 Tohoku–Oki earthquakes with apparent coefficients of (a) 0.1 and (b) 0.8. The vertical error bars indicate the standard deviation obtained through the Monte Carlo simulation.

Additional file 13: Figure S13. (a) Distribution of the Δ CFF calculated for the F-net focal mechanisms during the pre-seismic (left) and post-seismic (right) periods. The apparent coefficient of friction is assumed to be 0.1. (b) Temporal changes of the median Coulomb stress change for (a). The histograms for receiver faults during the pre-seismic and post-seismic periods are also shown.

Additional file 14: Figure S14. (a) Distribution of the Δ CFF calculated for the F-net focal mechanisms during the pre-seismic (left) and post-seismic (right) periods. The apparent coefficient of friction is assumed to be 0.8. (b) Temporal changes of the median Coulomb stress change for (a). The histograms for receiver faults during the pre-seismic and post-seismic periods are also shown.

Abbreviations

Δ CFF: static change in the Coulomb failure function; GCMT: global centroid moment tensor.

Authors' contributions

TI conceived the original concept of the present paper, performed the computations and analysis, and wrote the final manuscript. YO, HT, and KS provided suggestions to improve the research, supervised the writing of the manuscript, and approved the final version. All authors read and approved the final manuscript.

Author details

¹ Association for the Development of Earthquake Prediction, 1-5-18, Sarugaku-cho, Chiyoda-ku, Tokyo 101-0064, Japan. ² Earthquake Research Institute, the University of Tokyo, 1-1-1 Yayoi, Bunkyo-ku, Tokyo 113-0032, Japan. ³ The Institute of Statistical Mathematics, 10-3 Midori-cho, Tachikawa, Tokyo 190-8562, Japan.

Acknowledgements

The authors would like to thank Jian Wang and the anonymous reviewers for their helpful comments. The authors would also like to thank all of the organizations and individuals mentioned in the "Availability of data and materials" section, who provided the data and information used in the present study.

Competing interests

The authors declare that they have no competing interests.

Availability of data and materials

We used the Global Centroid Moment Tensor (GCMT) catalog (<http://www.globalcmt.org/CMTsearch.html>), last accessed October 2015) and F-net focal mechanism solutions provided by the National Research Institute for Earth Science and Disaster Resilience (NIED) (<http://www.fnet.bosai.go.jp/top.php?LANG=en>), last accessed November 2015) for receiver faults in calculating Coulomb stress changes. We also used Generic Mapping Tools (Wessel and Smith 1998) for drawing figures (<http://gmt.soest.hawaii.edu/>), last accessed January 2012), the TSEIS visualization package (Tsuruoka 1998) for the study of hypocenter data (<https://www.weic.eri.u-tokyo.ac.jp/db/index.html>), last accessed October 2015), and a subroutine program developed by Okada (1992) for calculating ΔCFF (http://www.bosai.go.jp/study/application/dc3d/DC3Dhtml_E.html), last accessed October 2015). Several fault-slip models for the 2004 Sumatra–Andaman, 2010 Maule, and 2011 Tohoku–Oki earthquakes are available from the online database of finite-fault rupture models (SRCMOD) (Mai and Thingbaijam 2014) (<http://equake-rc.info/SRCMOD/>), last accessed August 2016).

Funding

The present study was supported by the Ministry of Education, Culture, Sports, Science, and Technology of Japan under its Earthquake and Volcano Hazards Observation and Research Program and the Special Project for Reducing Vulnerability for Urban Mega-earthquake Disasters.

Received: 26 October 2016 Accepted: 10 February 2017

Published online: 06 March 2017

References

- Ammon CJ, Chen J, Thio H-K, Robinson D, Ni S, Hjorleifsdottir V, Kanamori H, Lay T, Das S, Helmberger D, Ichinose G, Polet J, Wald D (2005) Rupture process of the great 2004 Sumatra–Andaman earthquake. *Science* 308:1133–1139
- Anderson JG, Brune JN, Louie JN, Zeng Y, Savage M, Yu G, Chen Q, dePolo D (1994) Seismicity in the western Great Basin apparently triggered by the Landers, California, Earthquake, 28 June 1992. *Bull Seism Soc Am* 84(3):863–891
- Asano Y, Saito T, Ito Y, Shiomi K, Hirose H, Matsumoto T, Aoi S, Hori S, Sekiguchi S (2011) Spatial distribution and focal mechanisms of aftershocks of the 2011 off the Pacific coast of Tohoku Earthquake. *Earth Planets Space* 63(7):669–673. doi:10.5047/eps.2011.06.016
- Bird P (2003) An updated digital model of plate boundaries. *Geochem Geophys Geosyst* 4(3):1027. doi:10.1029/2001GC000252
- Byerlee JD, Brace WF (1968) Stick-slip stable sliding and earthquakes –effect of rock type, pressure, strain rate, and stiffness. *J Geophys Res* 73(18):6031–6037
- Chan C-H, Stein RS (2009) Stress evolution following the 1999 Chi-Chi, Taiwan, earthquake: consequences for afterslip, relaxation, aftershocks and departures from Omori decay. *Geophys J Int* 177(1):179–192. doi:10.1111/j.1365-246X.2008.04069.x
- Chan C-H, Wang Y, Almeida R, Yadav RBS (2016) Enhanced stress and changes to regional seismicity due to the 2015 Mw 7.8 Gorkha, Nepal, earthquake on the neighbouring segments of the Main Himalayan Thrust. *J Asian Earth Sci*. doi:10.1016/j.jseaeas.2016.03.004
- Delouis B, Nocquet JM, Vallée M (2010) Slip distribution of the February 27, 2010 Mw = 8.8 Maule Earthquake, central Chile, from static and high-rate GPS, InSAR, and broadband teleseismic data. *Geophys Res Lett* 37(17):L17305. doi:10.1029/2010GL043899
- Dewey JW, Choy G, Presgrave B, Sipkin S, Tarr AC, Benz H, Earle P, Wald D (2007) Seismicity associated with the Sumatra–Andaman Islands earthquake of 26 December 2004. *Bull Seism Soc Am* 97(1A):S25–S42. doi:10.1785/0120050626
- Ekström G, Nettles M, Dziewoński AM (2012) The global CMT project 2004–2010: centroid-moment tensors for 13,017 earthquakes. *Phys Earth Planet Inter* 200–201:1–9. doi:10.1016/j.pepi.2012.04.002
- Enescu B, Aoi S, Toda S, Suzuki W, Obara K, Shiomi K, Takeda T (2012) Stress perturbations and seismic response associated with the 2011 M9.0 Tohoku-oki earthquake in and around the Tokai seismic gap, central Japan. *Geophys Res Lett* 39(13):L00G28. doi:10.1029/2012GL051839
- Fariás M, Comte D, Roecker S, Carrizo D, Pardo M (2011) Crustal extensional faulting triggered by the 2010 Chilean earthquake: The Pichilemu Seismic Sequence. *Tectonics* 30:TC6010. doi:10.1029/2011TC002888
- Fujii Y, Satake K (2007) Tsunami source of the 2004 Sumatra–Andaman earthquake inferred from tide gauge and satellite data. *Bull Seism Soc Am* 97(1A):S192–S207. doi:10.1785/0120050613
- Fujii Y, Satake K (2013) Slip distribution and seismic moment of the 2010 and 1960 Chilean earthquakes inferred from tsunami waveforms and coastal geodetic data. *Pure Appl Geophys* 170(9):1493–1509. doi:10.1007/s00024-012-0524-2
- Fukuyama E, Ishida M, Dreger DS, Kawai H (1998) Automated seismic moment tensor determination by using on-line broadband seismic waveforms. *Zisin (J Seismol Soc Jpn) Ser. 2*(51):149–156 (in Japanese with English abstract)
- Gusman AR, Tanioka Y, Sakai S, Tsushima H (2012) Source model of the great 2011 Tohoku earthquake estimated from tsunami waveforms and crustal deformation data. *Earth Planet Sci Lett* 341–344:234–242
- Hardebeck JL, Nazareth JJ, Hauksson E (1998) The static stress change triggering model: constraints from two southern California aftershock sequences. *J Geophys Res* 103(B10):24427–24437
- Harris RA, Simpson RW (1992) Changes in static stress on southern California faults after the 1992 Landers earthquake. *Nature* 360:251–254. doi:10.1038/360251a0
- Heidarzadeh M, Harada T, Satake K, Ishibe T, Gusman AR (2016) Comparative study of two tsunamigenic earthquakes in the Solomon Islands: 2015 Mw 7.0 normal-fault and 2013 Santa Cruz Mw 8.0 megathrust earthquakes. *Geophys Res Lett* 43(9):4340–4349. doi:10.1002/2016GL068601
- Heki K, Mitsui Y (2013) Accelerated Pacific plate subduction following interplate thrust earthquakes at the Japan trench. *Earth Planet Sci Lett* 363:44–49. doi:10.1016/j.epsl.2012.12.031
- Hill DP, Reasenber PA, Michael A, Arabaz WJ, Beroza G, Brumbaugh D, Brune JN, Castro R, Davis S, dePolo D, Ellsworth WL, Gombert J, Harmsen S, House L, Jackson SM, Johnston MJS, Jones L, Keller R, Malone S, Munguia L, Nava S, Pechmann JC, Sanford A, Simpson RW, Smith RB, Stark M, Stickney M, Vidal A, Walter S, Wong V, Zollweg J (1993) Seismicity remotely triggered by the magnitude 7.3 Landers, California, earthquake. *Science* 260:1617–1623. doi:10.1126/science.260.5114.1617
- Hubbert MK, Rubey WW (1959) Role of fluid pressure in mechanics of overthrust faulting I. Mechanics of fluid-filled porous solids and its application to overthrust faulting. *Geol Soc Am Bull* 70(2):115–166. doi:10.1130/0016-7606(1959)70[115:ROFPIM]2.0.CO;2
- Imanishi K, Kuwahara Y, Takeda T, Haryu Y (2006) The seismicity, fault structures, and stress field in the seismic gap adjacent to the 2004 Mid-Niigata earthquake inferred from seismological observations. *Earth Planets Space* 58(7):831–841. doi:10.1186/BF03351988
- Ishibe T, Shimazaki K, Tsuruoka H, Yamanaka Y, Satake K (2011a) Correlation between Coulomb stress changes imparted by large historical strike-slip earthquakes and current seismicity in Japan. *Earth Planets Space* 63(3):301–314. doi:10.5047/eps.2011.01.008
- Ishibe T, Shimazaki K, Satake K, Tsuruoka H (2011b) Change in seismicity beneath the Tokyo metropolitan area due to the 2011 off the Pacific coast of Tohoku Earthquake. *Earth Planets Space* 63(7):731–735. doi:10.5047/eps.2011.06.001
- Ishibe T, Satake K, Sakai S, Shimazaki K, Tsuruoka H, Yokota Y, Nakagawa S, Hirata N (2015) Correlation between Coulomb stress imparted by the 2011 Tohoku–Oki earthquake and seismicity rate change in Kanto, Japan. *Geophys J Int* 201(1):112–134. doi:10.1093/gji/ggv001
- Kato A, Sakai S, Obara K (2011) A normal-faulting seismic sequence triggered by the 2011 off the Pacific coast of Tohoku Earthquake: wholesale stress regime changes in the upper plate. *Earth Planets Space* 63(7):745–748. doi:10.5047/eps.2011.06.014
- King GCP, Stein RS, Lin J (1994) Static stress changes and the triggering of earthquakes. *Bull Seism Soc Am* 84(3):935–953

- Konca AO, Hjørleifsdóttir V, Song TA, Avouac J, Helmberger DV, Ji C, Sieh K, Briggs R, Meltzner A (2007) Rupture kinematics of the 2005, Mw 8.6 Nias-Simeulue earthquake from the joint inversion of seismic and geodetic data. *Bull Seism Soc Am* 97(1):S307–S322. doi:[10.1785/0120050632](https://doi.org/10.1785/0120050632)
- Lay T, Kanamori H, Ammon CJ, Nettles M, Ward SN, Aster RC, Beck SL, Bilek SL, Brudzinski MR, Butler R, Deshon HR, Ekström G, Satake K, Sipkin S (2005) The great Sumatra–Andaman earthquake of 26 December 2004. *Science* 308(5725):1127–1133. doi:[10.1126/science.1112250](https://doi.org/10.1126/science.1112250)
- Luttrell KM, Tong X, Sandwell DT, Brooks BA, Bevis MG (2011) Estimates of stress drop and crustal tectonic stress from the 27 February 2010 Maule, Chile, earthquake: implications for fault strength. *J Geophys Res* 116(B11):B11401. doi:[10.1029/2011JB008509](https://doi.org/10.1029/2011JB008509)
- Mai PM, Thingbaijam KKS (2014) SRCMOD: an online database of finite-fault rupture models. *Seism Res Lett* 85(6):1348–1357. doi:[10.1785/0220140077](https://doi.org/10.1785/0220140077)
- Miao M, Zhu S-B (2012) A study of the impact of static Coulomb stress changes of megathrust earthquakes along subduction zone on the following aftershocks. *Chin J Geophys* 55(5):539–551
- Miyazawa M (2011) Propagation of an earthquake triggering front from the 2011 Tohoku-Oki earthquake. *Geophys Res Lett* 38(23):L23307. doi:[10.1029/2011GL049795](https://doi.org/10.1029/2011GL049795)
- Nettles M, Ekström G, Koss HC (2011) Centroid-moment-tensor analysis of the 2011 off the Pacific coast of Tohoku Earthquake and its larger foreshocks and aftershocks. *Earth Planets Space* 63(7):519–523. doi:[10.5047/eps.2011.06.009](https://doi.org/10.5047/eps.2011.06.009)
- Ogata Y (2007) Seismicity and geodetic anomalies in a wide area preceding the Niigata-Ken-Chuetsu earthquake of 23 October 2004, central Japan. *J Geophys Res* 112(B10):B10301. doi:[10.1029/2006JB004697](https://doi.org/10.1029/2006JB004697)
- Okada Y (1992) Internal deformation due to shear and tensile faults in a half space. *Bull Seism Soc Am* 82(2):1018–1040
- Pollitz FF, Sacks IS (1995) Consequences of stress changes following the 1891 Nobi earthquake, Japan. *Bull Seism Soc Am* 85(3):796–807
- Reasenber PA, Simpson RW (1992) Response of regional seismicity to the static stress change produced by the Loma Prieta earthquake. *Science* 255(5052):1687–1690. doi:[10.1126/science.255.5052.1687](https://doi.org/10.1126/science.255.5052.1687)
- Rhie J, Dreger D, Bürgmann R, Romanowicz B (2007) Slip of the 2004 Sumatra–Andaman earthquake from joint inversion of long-period global seismic waveforms and GPS static offsets. *Bull Seism Soc Am* 97(1A):S115–S127. doi:[10.1785/0120050620](https://doi.org/10.1785/0120050620)
- Satake K, Fujii Y, Harada T, Namegaya Y (2013) Time and space distribution of coseismic slip of the 2011 Tohoku earthquake as inferred from tsunami waveform data. *Bull Seism Soc Am* 103(2B):1473–1492. doi:[10.1785/0120120122](https://doi.org/10.1785/0120120122)
- Skempton AW (1954) The pore pressure coefficients A and B. *Geotechnique* 4(4):143–147. doi:[10.1680/geot.1954.4.4.143](https://doi.org/10.1680/geot.1954.4.4.143)
- Stein RS, King GCP, Lin J (1992) Change in failure stress on the southern San Andreas fault system caused by the 1992 Magnitude = 7.4 Landers earthquake. *Science* 258(5086):1328–1332. doi:[10.1126/science.258.5086.1328](https://doi.org/10.1126/science.258.5086.1328)
- Stein RS, King GCP, Lin J (1994) Stress triggering of the 1994 M = 6.7 Northridge, California, earthquake by its predecessors. *Science* 265(5177):1432–1435. doi:[10.1126/science.265.5177.1432](https://doi.org/10.1126/science.265.5177.1432)
- Toda S (2008) Coulomb stresses imparted by the 25 March 2007 Mw = 6.6 Noto-Hanto, Japan, earthquake explain its ‘butterfly’ distribution of aftershocks and suggest a heightened seismic hazard. *Earth Planets Space* 60(10):1041–1046. doi:[10.1186/BF03352866](https://doi.org/10.1186/BF03352866)
- Toda S, Stein RS (2013) The 2011 M = 9.0 Tohoku oki earthquake more than doubled the probability of large shocks beneath Tokyo. *Geophys Res Lett* 40(11):2562–2566. doi:[10.1002/grl.50524](https://doi.org/10.1002/grl.50524)
- Toda S, Stein RS, Reasenber PA, Dieterich JH, Yoshida A (1998) Stress transferred by the 1995 Mw = 6.9 Kobe, Japan, shock: effect on aftershocks and future earthquake probabilities. *J Geophys Res* 103(B10):24543–24565. doi:[10.1029/98JB00765](https://doi.org/10.1029/98JB00765)
- Toda S, Lin J, Stein RS (2011) Using the 2011 Mw 9.0 off the Pacific coast of Tohoku Earthquake to test the Coulomb stress triggering hypothesis and to calculate faults brought closer to failure. *Earth Planets Space* 63(7):725–730. doi:[10.5047/eps.2011.05.010](https://doi.org/10.5047/eps.2011.05.010)
- Tsuruoka H (1998) Development of seismicity analysis software on workstation. *Tech Res Rep ERI Univ Tokyo* 2:34–42 (in Japanese with English abstract)
- Uchida N, Asano Y, Hasegawa A (2016) Acceleration of regional plate subduction beneath Kanto, Japan, after the 2011 Tohoku-oki earthquake. *Geophys Res Lett* 43(17):9002–9008. doi:[10.1002/2016GL070298](https://doi.org/10.1002/2016GL070298)
- Wessel P, Smith WHF (1998) New, improved version of generic mapping tools released. *EOS Trans AGU* 79(47):579. doi:[10.1029/98EO00426](https://doi.org/10.1029/98EO00426)
- Woessner J, Jónsson S, Sudhaus H, Baumann C (2012) Reliability of Coulomb stress changes inferred from correlated uncertainties of finite-fault source models. *J Geophys Res* 117(B7):B07303. doi:[10.1029/2011JB009121](https://doi.org/10.1029/2011JB009121)
- Yokota Y, Koketsu K, Fujii Y, Satake K, Sakai S, Shinohara M, Kanazawa T (2011) Joint inversion of strong motion, teleseismic, geodetic, and tsunami datasets for the rupture process of the 2011 Tohoku earthquake. *Geophys Res Lett* 38(7):L00G21. doi:[10.1029/2011GL050098](https://doi.org/10.1029/2011GL050098)

Submit your manuscript to a SpringerOpen® journal and benefit from:

- Convenient online submission
- Rigorous peer review
- Immediate publication on acceptance
- Open access: articles freely available online
- High visibility within the field
- Retaining the copyright to your article

Submit your next manuscript at ► springeropen.com